Review Article

Annie Shalom Isaac* and Cornelius Neumann

Optimization of freeform surfaces using intelligent deformation techniques for LED applications

https://doi.org/10.1515/aot-2017-0074
Received November 10, 2017; accepted February 25, 2018; previously published online March 22, 2018

Abstract: For many years, optical designers have great interests in designing efficient optimization algorithms to bring significant improvement to their initial design. However, the optimization is limited due to a large number of parameters present in the Non-uniform Rationaly b-Spline Surfaces. This limitation was overcome by an indirect technique known as optimization using freeform deformation (FFD). In this approach, the optical surface is placed inside a cubical grid. The vertices of this grid are modified, which deforms the underlying optical surface during the optimization. One of the challenges in this technique is the selection of appropriate vertices of the cubical grid. This is because these vertices share no relationship with the optical performance. When irrelevant vertices are selected, the computational complexity increases. Moreover, the surfaces created by them are not always feasible to manufacture, which is the same problem faced in any optimization technique while creating freeform surfaces. Therefore, this research addresses these two important issues and provides feasible design techniques to solve them. Finally, the proposed techniques are validated using two different illumination examples: street lighting lens and stop lamp for automobiles.

Keywords: curvature; freeform deformation; freeform optics; illumination; LED; optimization.

1 Introduction

The growth of freeform optics is dramatic during the last 10 years. The design of freeform optics relies heavily on one of the methods: tailoring based on point source assumption [1, 2], SMS design [3], and source target maps based on equal flux grids [4] to create an initial optical surface. However, these results are not always guaranteed to yield optimal performance when extended light sources are used. This is because finding a ray transformation to yield a continuous refractive or reflective surface is challenging for complicated source representation. Therefore, optical designers still need to rely on any optimization technique to improve their design to meet the target requirements [5–7]. In order to effectively use optimization for freeform surfaces, parameterization of surfaces is essential to reduce the number of optimization variables. This is achieved using a method known as optimization using freeform deformation (OFFD) proposed by Wendel et al. [8]. This contribution addresses two important issues present in the OFFD. The first one is finding the relationship between the cubical grid and the photometric performance, and the second one is the implementation of the manufacturing feasibility analysis in the OFFD. So this work is organized as follows. The freeform deformation (FFD) optimization technique is elaborated in detail in the Section 2. This section also explains the limitations of this work and introduces the proposed design techniques. Section 3 addresses the design techniques to establish the relationship between the grid and the target distribution, and Section 4 provides the manufacturing feasibility analysis. Section 5 provides the implementation of these techniques in the OFFD system, and these are validated using street lighting lens as an example in Section 6 and automotive stop lamps in Section 7, respectively. Finally, it ends with a conclusion in Section 8.

2 Optimization using freeform deformation technique

2.1 State-of-the-art

The OFFD method employs the FFD technique proposed by Sederberg [9] coupled with an optimization routine.

***Corresponding author: Annie Shalom Isaac,** Scientific Staff, Light Technology Institute, Karlsruhe Institute of Technology, Engesserstrasse 13, Karlsruhe 76131, Germany, e-mail: annie.chandra@kit.edu
Cornelius Neumann: Light Technology Institute, Karlsruhe Institute of Technology, Engesserstrasse 13, Karlsruhe 76131, Germany

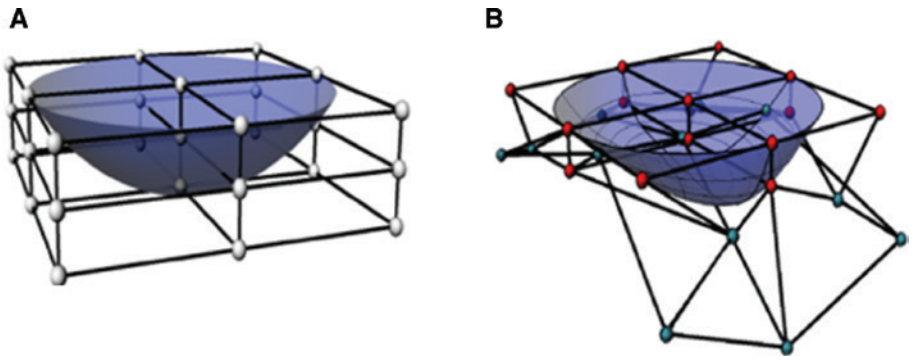

Figure 1: Cubical grid enclosing the optical surface (A) before and (B) after deformation.

The relationship between the grid and the optical surface is established using the FFD algorithm [9]. In this method, the optical surface is first placed in a parallelepiped grid. The control points of the grid are then pushed in or pulled out, and this effect is transmitted to the underlying optical surface. The mathematical techniques described by the FFD algorithm provide deformation to the optical surface when the control points of the grid are modified. Figure 1 shows an example of the grid enclosing a spherical surface before and after deformation.

The algorithm as explained in the flowchart in Figure 2 begins with an input surface whose optical performance needs to be improved. The optical surface is placed inside the grid whose vertices are known as grid points. A combination of grid points are selected as optimization variables, and the optimization algorithm is then free to provide displacements along all the directions of the enclosed grid. As the enclosed grid changes during the optimization, the underlying optical surface changes, respectively, as specified in the FFD algorithm. The deformed surface is then evaluated photometrically, and based on this result, the optimization algorithm continues until the target lighting requirements are met. The Nelder-Mead simplex technique is used as its optimization algorithm [10].

The main role in modifying the shape of the optical surface is achieved using the FFD technique [8]. As a first step in this FFD technique, the optical surface will be mapped to a rectangular lattice space by a coordinate transformation. This is defined in terms of a tensor product trivariate Bernstein polynomial. In the next step, the rectangular grid points have to be computed based on the size of the optical surface. The third step is the deformation step, which can be attained by specifying the displacement values to the grid control points. As a last step, this deformation of the grid causes deformation of the underlying surface and the coordinates of the new surface, and this can be obtained by again evaluating the Bernstein polynomial.

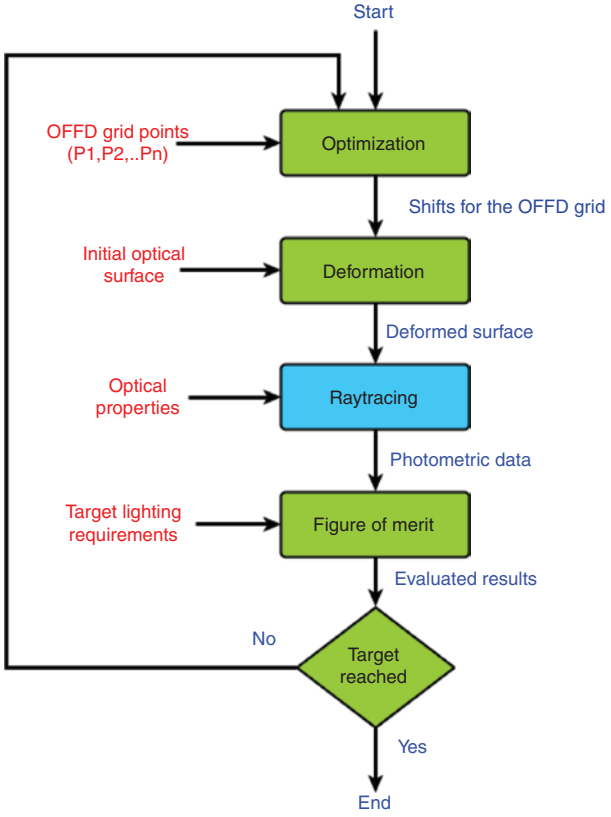

Figure 2: Workflow showing the optimization using freeform deformation technique (OFFD).

The optical performance is then characterized using a commercial standard ray tracer and evaluated using deviation-based and flux-based merit functions based on the design objective.

The deviation-based merit function evaluates how far the actual distribution varies from the desired lighting requirements. In this method, Q_{dev} is calculated by evaluating the deviation of each corresponding pixel (x) between the current and the desired distribution, which can be expressed in Eq. (1).

$$Q_{\text{dev}} = \int_G [E_{\text{ideal}}(x) - E(x)]^2 \, dx, \tag{1}$$

where G is the target area one is interested in, $E_{\text{ideal}}(x)$ is the desired illuminance or intensity distribution, and $E(x)$ is the current distribution. On the contrary, the luminous flux-based merit function evaluates Q_{flux} by comparing the total luminous flux in the target area φ_{target} of the current system with the total flux available from the light source φ_{source}. Q_{flux} is calculated using Eq. (2).

$$Q_{\text{flux}} = 1 - \frac{\varphi_{\text{target}}}{\varphi_{\text{source}}}. \tag{2}$$

2.1.1 Limitation 1: grid complexity

The main challenge in the OFFD is the selection of grid points for the optimization algorithm. This is difficult because there is no relationship between the cubic OFFD grid and the target light distribution. So far, this has been done using the trial and error approach, or the grid points are selected based on the experience of the optical designer. Moreover, the selection of grid points is sensitive to target requirements, initial design, and its type (refractive or reflective). When such relationship is established, the OFFD can find the best possible grid vertices on its own, and the optimization is also guaranteed to attain the desired photometric requirements using these vertices in a short time. The method to find the best possible grid points is explained in Section 3.

2.1.2 Limitation 2: manufacturing feasibility of surfaces

In OFFD, the optimization algorithm provides shifts to the selected grid points along its three directions (x, y, z). This leads to the creation of some surfaces that cannot be manufactured. Some of the results produced by the OFFD are shown in Figure 3. This challenges the optical designer as the final optimized result is not always guaranteed to be manufactured, and each ray trace that is encountered in the infeasible surface is computationally irrelevant and consumes time. Section 4 provides a solution to this by implementing a surface analysis tool in the OFFD system.

3 Automatic selection of grid points

3.1 Challenges in the grid

The three-dimensional (3D) OFFD grid as seen in Figure 4 can be represented using n grid points marked as circles. A simple cubic grid can be constructed minimally using 27 vertices, and these vertices, called grid points, can be selected as the optimization variables in any arbitrary combination in search of the best possible solution. So there are a total of $27C_1 + 27C_2 + \cdots + 27C_{27} = 134217727$ combinations when calculated using ${}^{n}C_{r}$, where n is the total number of grid points, and r is the number of grid points selected without repetition. The combination set is so large that it could take years to search for the best optical surface if one follows a naive approach. So this complexity has to be eliminated using an appropriate design technique to select the optimal grid points in short duration.

3.2 Proposed approach

This technique follows a direct and discrete approach called as shift and scan technique, and its workflow is depicted in the flowchart shown in Figure 5. The light distribution (illuminance or intensity distribution) created by the initial surface is divided into an arbitrary number of segments, and the integrated luminous flux at each segment is calculated.

As expected, some segments of the distribution meet the desired lighting requirements and some others not because of the extension of the light source or the shape of the initial optics. So this step of evaluation is highly necessary to identify the segments (area of the distribution)

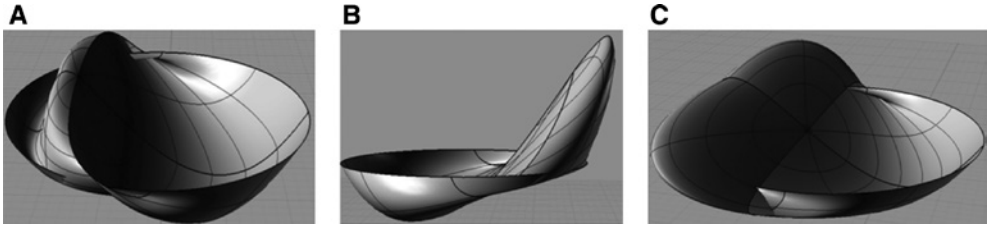

Figure 3: Examples of infeasible surfaces (A–C) generated by OFFD when optimizing the street lighting lens.

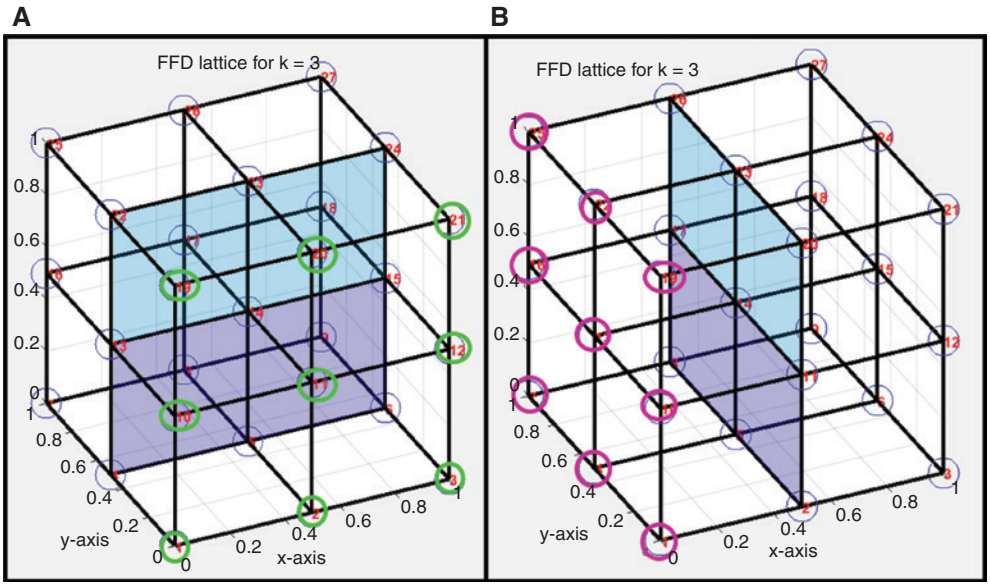

Figure 4: 3D OFFD grid showing (A) y symmetry marked with green circles and (B) x symmetry in magenta circles. The grid symmetricity ensures that one half of the grid is sufficient during the selection of the grid points [11].

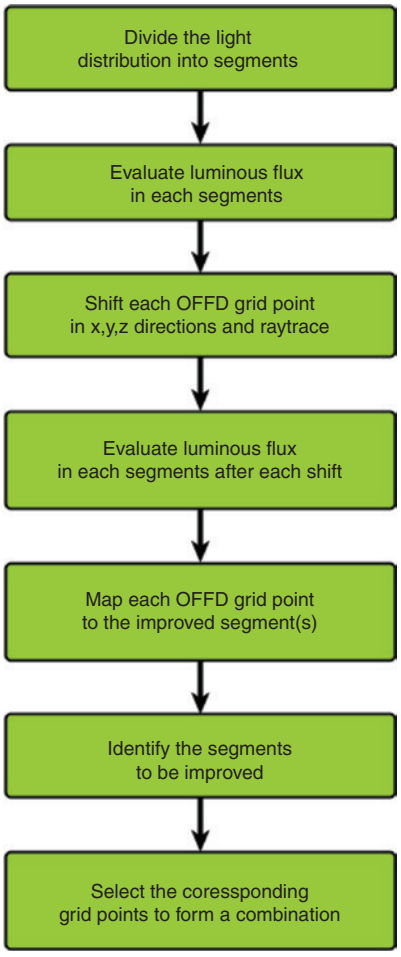

Figure 5: Flowchart showing the shift and scan technique used to select the grid points.

that must be improved. Then, the next step is to find the relationship between these segmented light distribution and the control points of the grid. As the grid control points or even the underlying optical surface do not share any prior relationship, this can be attained by shifting each single OFFD grid point along the x, y, and z directions, respectively. This shift will be transferred to the underlying optical surface and, in turn, will be reflected in the light distribution during the ray trace. During this step, it will be noticed that some segments perform better, and some get worse, and no change for others depending on the OFFD grid point. This performance measure (e.g. more luminous flux in the distribution) of each segment in response to a particular OFFD grid point is stored as a look-up table. From these results, the segments that need improvement and its corresponding OFFD grid points that could improve them are identified. These grid points form a combination and can be given as optimization variables to the OFFD later.

The extension of the shift depends on the initial surface and the demands of the modification. If the initial surface is far away from the target and significant modification of the optical surface is required, then the shift step size has to be selected larger or vice versa. The total number of segments and its size are completely at the discretion of the optical designer, and there is no specific restriction on it. Segments can be divided small or large based on the lighting requirements and the optical performance of the initial system. If the objective is to attain homogeneous light distribution, then uniform segmentation is more

meaningful. For certain tasks like automotive headlamp design, the angular lighting requirements differ throughout the region. For such requirements, non-uniform segmentation performs better. After this implementation, the initial guess or experience needed to select the optimization variables is eliminated. The optical designer does not need to define OFFD grid points as inputs anymore. It has been integrated as a part of the OFFD system by establishing a suitable grid-target relationship.

4 Manufacturing feasibility analysis of the surfaces

In any freeform surface, manufacturing is restricted mostly based on its curvature and size. By designing a suitable surface analysis tool, which analyzes the curvature and size of the generated optical surface, infeasible surfaces can be restricted by adding suitable tolerance limits. This section explains how this analysis is carried out and integrated as a part of the OFFD system.

4.1 Curvature analysis

The Gaussian curvature helps us to show anomalies in the curvature of a surface like bumps, dents, ripples, or areas that exhibit high or low curvature than the surrounding ones [12]. For an object in 3D space, there is always a tangent plane to that surface at a specific point (u, v). The normal curvature sections can be then computed for all directions to this tangent plane. From these, two surface curves crossing this point (u, v) are selected: one with maximum curvature κ_1 and the other with minimum curvature κ_2 as shown in Figure 6. The Gaussian curvature of a regular tensor product parametric B-spline surface $S(u, v)$ denoted by κ is the product of κ_1 and κ_2 [12–16] as shown in Eq. 3.

$$\kappa(u,v) = \kappa_1(u,v) \times \kappa_2(u,v). \tag{3}$$

The surface normal $n(u, v)$ is given by

$$n(u,v) = \frac{S_u \times S_v}{\| S_u \times S_v \|}. \tag{4}$$

The subscripts S_u and S_v indicate the partial derivatives with respect to the corresponding parameters u and v, respectively. The matrix representation of the first fundamental form of the surface is given by:

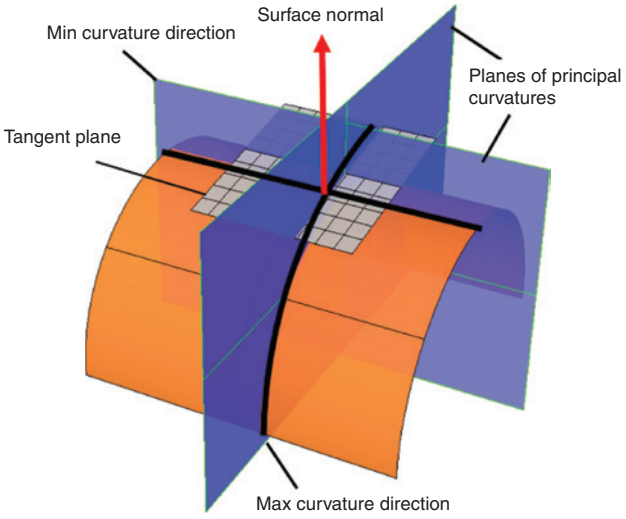

Figure 6: Schematic representation of the NURBS (orange) with a tangent plane (gray) cut by planes of principal curvatures (blue).

$$I = \begin{bmatrix} E & F \\ F & G \end{bmatrix} = \begin{bmatrix} \langle S_u, S_u \rangle & \langle S_u, S_v \rangle \\ \langle S_u, S_v \rangle & \langle S_v, S_v \rangle \end{bmatrix}, \tag{5}$$

and the matrix representation of the second fundamental form is given by:

$$II = \begin{bmatrix} L & M \\ M & N \end{bmatrix} = \begin{bmatrix} \langle S_{uu}, n \rangle & \langle S_{uv}, n \rangle \\ \langle S_{uv}, n \rangle & \langle S_{vv}, n \rangle \end{bmatrix}. \tag{6}$$

Let A, B, and C be defined as follows:

$$A = EG - F^2;\ B = 2FM - GL - EN;\ C = LN - M^2.$$

Now, the principal curvatures at a point on the surface is given by:

$$\kappa_1 = \frac{-B + \sqrt{B^2 - 4AC}}{2A};\ \kappa_2 = \frac{-B - \sqrt{B^2 - 4AC}}{2A}\ \kappa_1 \geq \kappa_2.$$

By substituting the suitable partial derivatives for A, B, and C and solving the equation, it gets simplified to

$$\kappa = \frac{LN - M^2}{EG - F^2}. \tag{7}$$

$\kappa(u, v)$ is determined as a function value for each section of the Non-uniform Rationaly b-Spline Surfaces (NURBS) patch whose interval is limited by knot vectors. For a NURBS with n knot vectors along the u direction and m knot vectors in the v direction, the Gaussian curvature $\kappa(u, v)$ has to be evaluated for a total of $n \times m$ points. The range of these curvature values can be specified as tolerance limits to the optimization algorithm. The information regarding the range of curvature values can be obtained from optical manufacturers.

4.2 Size analysis

Once the curvature analysis of the optical surface is over, its size has to be checked. The size analysis can be either diameter, thickness, minimum or maximum allowable source-optics distance, or even overall size of an optical surface. By specifying these parameters as limits along the three directions (x, y, z), the arbitrary change in shape of the freeform surface is restricted.

4.3 Proposed approach

The range of curvature values and optics dimensions are set as threshold values to the OFFD. Then, the curvature and its size are analyzed for the entire domain of the NURBS surface, and an $n \times m$ analysis matrix is created. This matrix is compared against the threshold values. If it is less or equal, then the surface is allowed for ray tracing and photometric evaluation. If it does not satisfy, then this surface is discarded, and the algorithm re-iterates back to the optimization to search and create new optimization variables. This is established using a non-smooth penalty-based binary approach in which the optimization is allowed to continue if the curvature and size are well within its limits and, it is represented in Eq. (8). If it exceeds, the value of the merit function governing them is increased to the maximum limit.

$$Q = \mu_{\text{pho}} Q_{\text{pho}} + \mu_{\text{geo}}, \tag{8}$$

where μ_{pho} and μ_{geo} govern the geometric and the photometric requirements, respectively. μ_{geo} remains zero, and

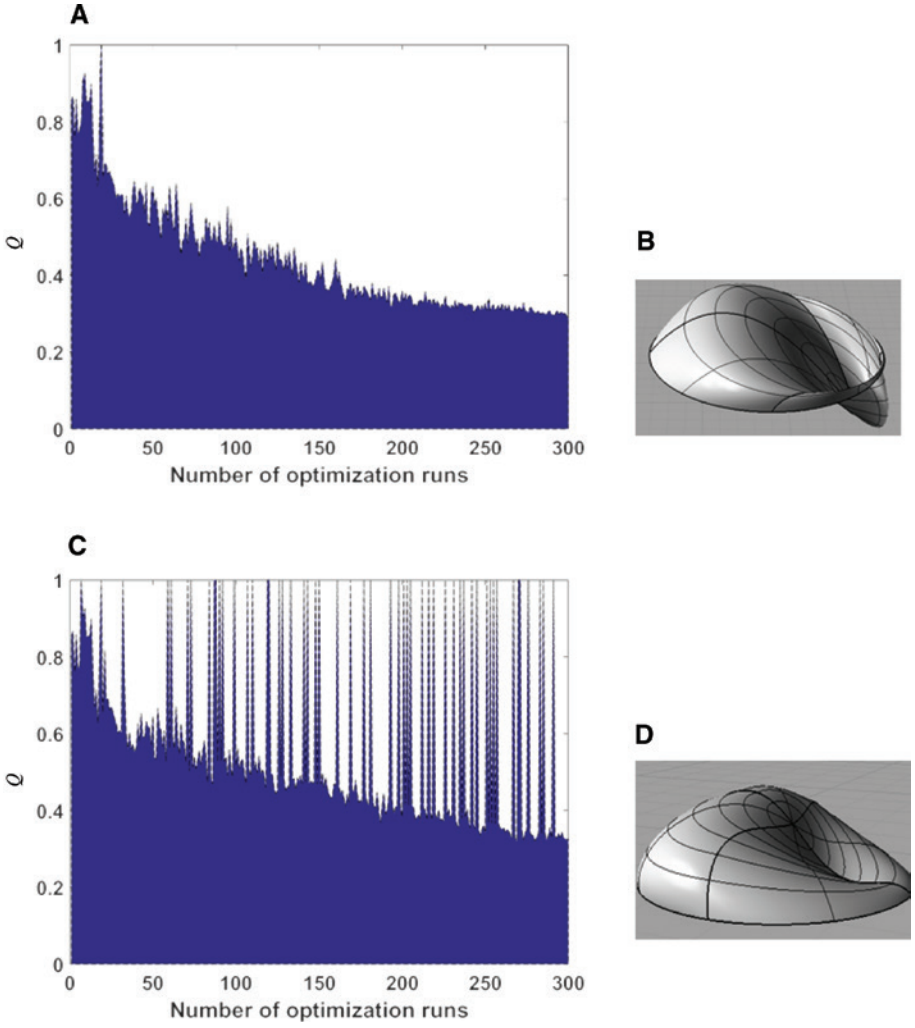

Figure 7: (A) Q landscape of the evaluated merit function based only on photometric evaluation, (B) deformed infeasible street lighting lens obtained as a result, (C) Q landscape when penalty based merit function based on Eq. (8) is used, and (D) deformed surface suitable to manufacture as well as satisfying the photometric requirements obtained as a result.

μ_{pho} is assigned to one if the surface is suitable to manufacture, and Q is, therefore, as a result of its evaluated photometric measure, Q_{pho}. When the system encounters any infeasible surface, the penalty parameter μ_{geo} is increased to one, and as ray tracing and photometric evaluation are not performed for such surfaces, the parameter μ_{pho} is assigned a zero. By doing so, the Q reaches to one, which is its maximum limit. Figure 7 shows the landscape of the evaluated Q when the merit functions based only on the photometric performance as in Ref. [11] and when penalty-based merit functions as described in Eq. (8) is used. The spotted peaks in the landscape are the instances when the infeasible surfaces are detected by the system, and these surfaces are not computed further. The Q progression is continued until a surface satisfying both the photometric and geometric measures as shown in Figure 7D is obtained.

5 Implementation of intelligent OFFD

The new techniques discussed in the previous sections, Sections 3 and 4, are included in the OFFD system, which is represented using a flowchart in Figure 8. The first step is to find optimal grid points to provide as variables to the optimization algorithm. This is achieved using the techniques elaborated in Section 3 and compressed as a single toolbox shown in pink. Then, the optimization algorithm provides shifts to deform the OFFD grid, which creates a new surface guided by the deformation algorithm. The newly generated surface is then checked for manufacturing feasibility using the size and curvature analysis tools as specified in Section 4. If the surface is suitable to manufacture, ray tracing is performed followed by a photometric evaluation. When the surface is detected as infeasible, it iterates back to the optimization and obtains new shifts, and hence, a new surface will be generated. This process continues until a surface suitable to manufacture and satisfying photometric requirements is created.

6 Validation using street lighting system

The setup of the street lighting design task is shown in Figure 9. Cree XPG2 LED (Cree, NC, USA) [17] with 100 lumens is used as a light source, and the initial spherical surface is shown in Figure 10. The efficiency of the initial

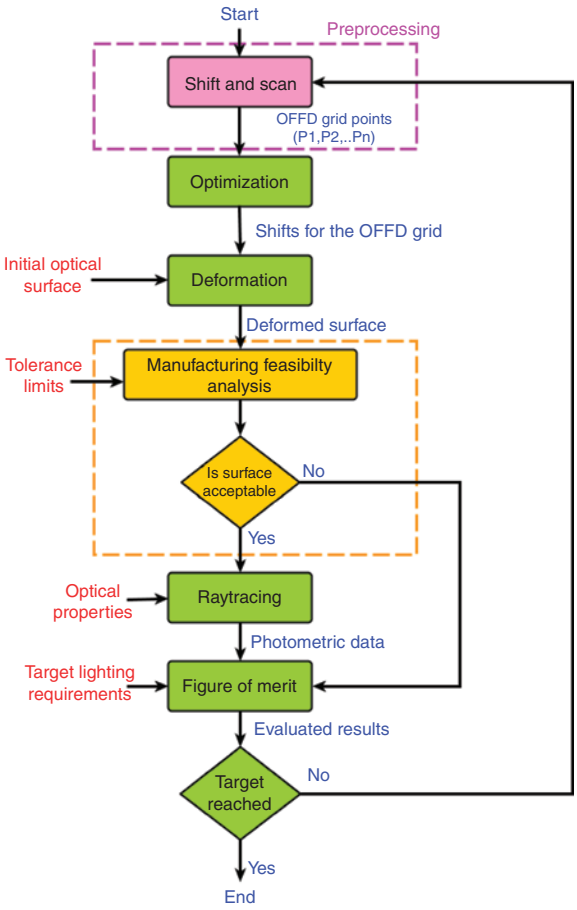

Figure 8: Flowchart showing the intelligent OFFD system with the newly integrated pre-processing step (pink) and manufacturing feasibility analysis (yellow).

surface η_{ini}, the total luminous flux redirected to the needed area, is only around 15.4%. Moreover, the shape of the initial distribution is far away from the target distribution

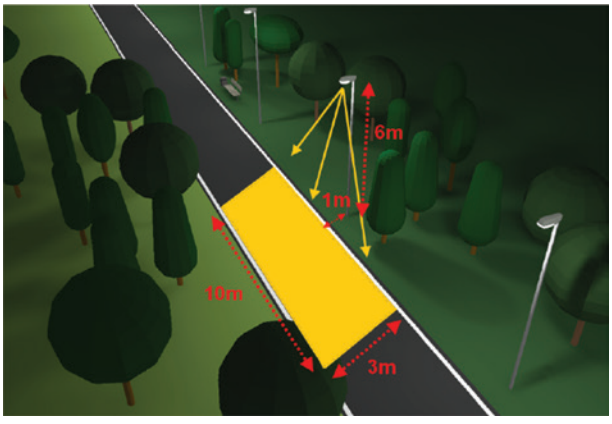

Figure 9: Schematic view of the street lighting setup with 10-m pole spacing, 6-m pole height, 1-m distance away from the road. The yellow rectangle shows the area to be illuminated [11].

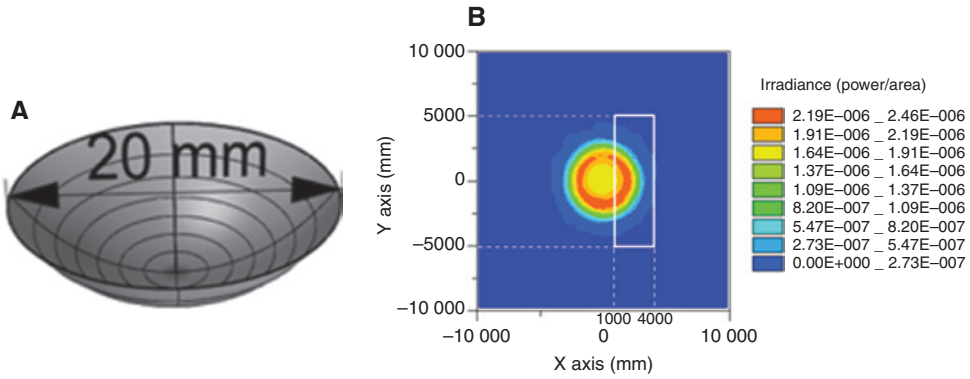

Figure 10: (A) Initial optical surface used for optimization of the street lighting system and (B) the illuminance distribution with a white rectangle showing the target distribution.

(marked as a white rectangle) as seen in Figure 10. This section shows how this optical surface gets optimized using the above-proposed techniques in the OFFD system.

6.1 Implementation results

The grid points can be selected using the technique described in Section 3. To begin with, the illuminance distribution is split into small segments. As this street lighting distribution is *y*-symmetric, it is sufficient to consider one-half of the OFFD grid, and the results can be mirrored to the other. The lower half (highlighted using pink dotted lines) is considered as seen in Figure 11A. It is clear that segments that are shown in turquoise (segments 2 and 3) and green (segments 1 and 6) require improvement. Once the segments are split and analyzed, the OFFD grid points that could improve these segments are figured out using the shift and scan technique stated in Section 3.2. The OFFD grid points found from the shift and scan step

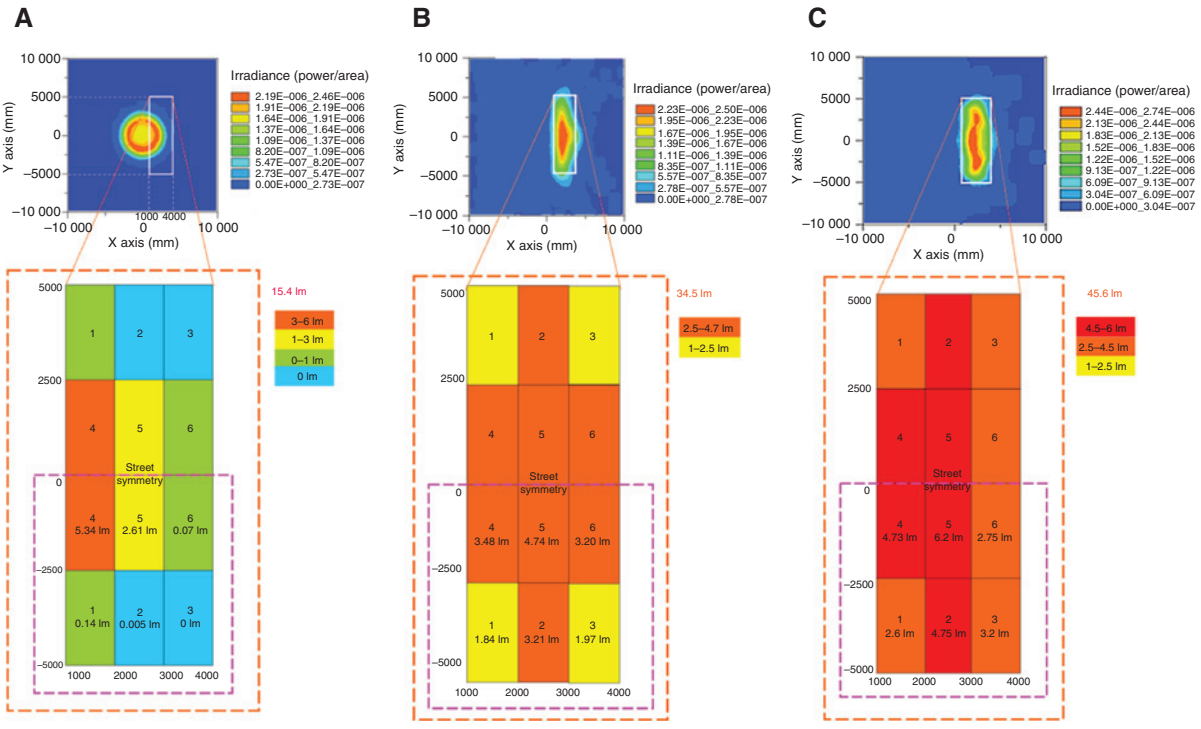

Figure 11: (A) Illuminance distribution of initial surface for the street lighting lens with the target being split into 12 segments and evaluated flux contribution at each segment; (B) first optimization results showing improved luminous flux in each segment; (C) second and final optimized results after 600 iterations.

are given as optimization variables to the OFFD, and optimization is carried out using the deviation-based merit function as in Eq. (1).

After the optimization, the light distribution is examined again for its improvement. From Figure 11B, it is seen that segments 1, 2, 3, and 6 have improved significantly, but still, segments 1 and 3 have to be improved further relative to others. So the shift and scan step is carried out again with respect to the newly generated optical surface, and a new map between the grid and the target is generated. The OFFD grid points that could improve segments 1 and 3 are found, and the surface is optimized again with these new OFFD grid points as optimization variables using flux-based merit function, and the final optimized results are obtained as in Figure 11C.

During this optimization process, the manufacturing feasibility analysis tool detected surfaces that cannot be manufactured. Some examples of such surfaces are shown in Figure 12. The first surface shown in Figure 12A is the initial spherical surface before optimization and exhibits positive curvature as expected. As the surface gets slowly deformed, the surface begins to exhibit more positive as well as negative curvatures based on the deformation of the OFFD grid. The surfaces from Figure 12A–C are well within the limit, and these surfaces could be manufactured, which is evident when one examines these surfaces visually. As the deformation of the grid becomes stronger and stronger, its impact on the optical surface gets higher, which is evident from Figure 12G–I where the positive or negative curvature increases tremendously and a substantial increase in the thickness, too. The surfaces in Figure 12D–I are discarded during the optimization as the evaluated parameters lie beyond the threshold. During this situation, the OFFD re-iterates back to get a feasible surface as seen in the flowchart in Figure 8.

6.2 Performance analysis

The optimization was performed using deviation-based merit function for 300 iterations followed by a flux-based function for 300 iterations. However, because of this new implementation, 116 surfaces are detected as infeasible ones and are not further computed. The optical efficiency of the distribution came around 45.8% leading to the same improvement of 30.4% as shown by the previous work [11]. In a standard four-core 3.30-GHz machine, the previous OFFD required 209 min to finish the entire process with a need of high expertise to select the optimal grid points at the beginning of the routine and manual intervention to detect infeasible surfaces. On the contrary, the intelligent OFFD required a total of 628 iterations, which include the ray traces being carried during its preprocessing step to select the appropriate grid points to attain the same results. It took 4 min to perform the preprocessing and 56 min for the optimization, which comes to a total of just

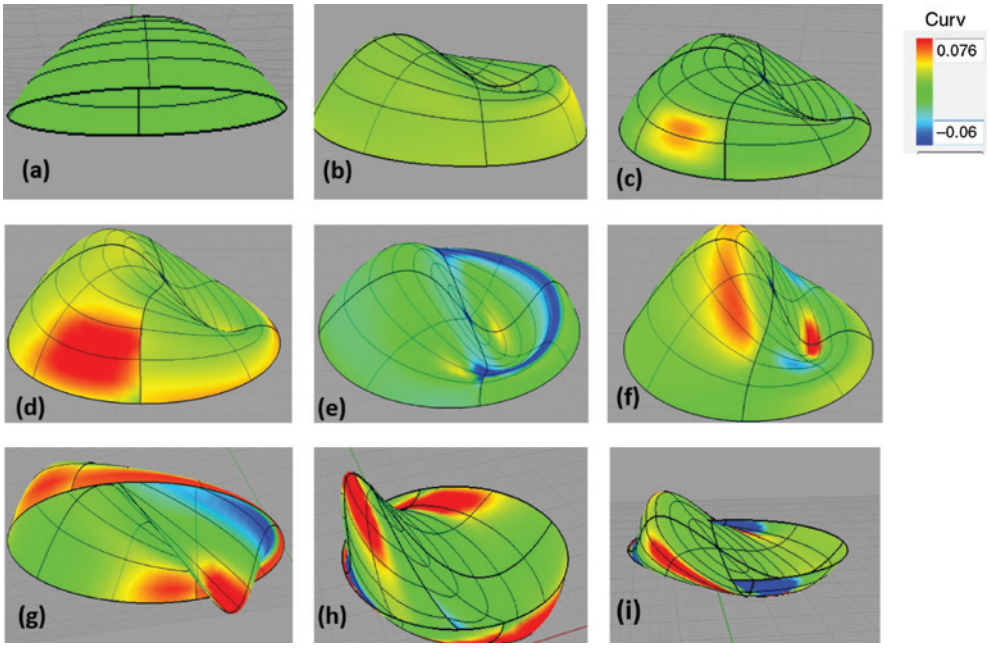

Figure 12: Examples of deformed surfaces for the street lighting lens detected by the intelligent OFFD during the manufacturing feasibility analysis.

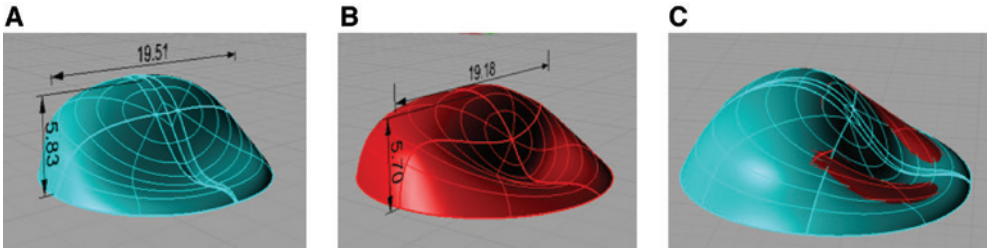

Figure 13: Deformed optical surface using (A) previous OFFD [11], (B) intelligent OFFD, and (C) the false color representation showing a minimal change in shape between them with all dimensions in millimeters.

Table 1: Comparison chart of the previous work [11] and the intelligent OFFD.

Parameters	Previous work [11]	Intelligent OFFD
Autonomous	No	Yes
Elimination of prior knowledge of grid	No	Yes
No. of. iterations	1500	628
Efficiency improvement	30.2%	30.4%
Time required (min)	209	60

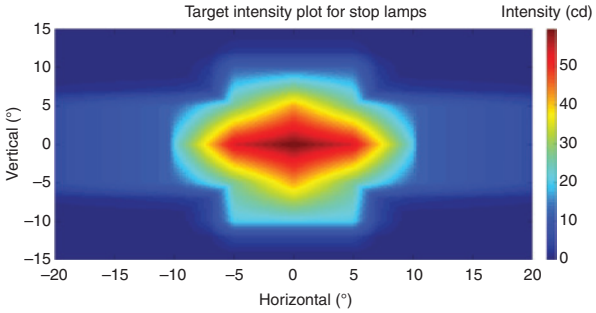

Figure 14: Interpolated target intensity distribution for stop lamp based on ECE R7 S1 [18].

an hour to complete this entire task in the same machine, which is almost 209/60 = 3.5 times faster than the previous OFFD. The optical surface generated by the intelligent OFFD, as shown in Figure 13, is almost similar to the previous OFFD, thereby, proving that an intelligent OFFD could find the best possible optical surface at a faster rate autonomously using its imparted intelligence. The performance measures are summarized in Table 1. The reason for its improvement in speed is due to the selection of the appropriate grid points using the preprocessing technique and allowing only feasible surfaces to perform ray tracing. More importantly, the intelligent OFFD does not require any prior knowledge about the OFFD grid points, and it finds them on the run, which eliminates the manual intervention completely.

7 Validation using stop lamps for automobiles

As a second example to show the potentiality of this work, the automotive stop lamp has been taken. The minimum intensities needed to fulfill the Economic Commission for Europe (ECE) standard [18] when designing stop lamps for automobiles are interpolated to create a target distribution as shown in Figure 14.

Luxeon Rebel LED from Lumileds, Amsterdam, Netherlands [19] with 20 lumens is taken as a light source, and the initial TIR optics with its intensity distribution is shown in Figure 15. From the intensity distribution, it is seen that it is collimated with high intensities around –2° until +2° and 810 candelas in the main beam direction (0°). This means this distribution fails to satisfy the ECE requirements because of its high intensity at the middle and less flux elsewhere. It is also to be noted that 95% of the collected luminous flux lies inside the needed target area as opposed to the street lighting lens. So optimization is not required to maximize the flux in the target, but the extra luminous flux in the middle must be optimally redirected throughout the target based on the legal requirements.

7.1 Implementation results

From the specifications given in the ECE standard, the intensity requirements needed for the stop lamp can be separated into two parts. The high-intensity requirements lies in the region –5° until +5° vertically and –10° until 10° horizontally, and the low-intensity at the outer edges needs to be at –15° until +15° vertically and –45° until 45° horizontally. So the optimization can be carried as two steps. The first one is to redistribute the luminous flux optimally in the high-intensity region, and the second one is to obtain the luminous flux in the low-intensity regions. When observing the target distribution

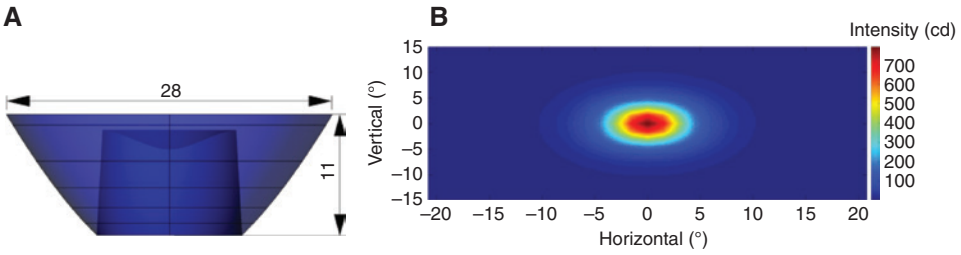

Figure 15: (A) Initial TIR hybrid optics for stop lamp and (B) its intensity distribution.

in Figure 14, it has both (horizontal and vertical) symmetries, and so the OFFD grid points must be selected accordingly.

To begin with, the intensity distribution is split into eight segments marked as 1, 2, 3, …, 8 as shown in Figure 16. The segments in the middle with high intensity are divided into small segments, while the segments that are far away from the middle are quite large. This uneven segmentation is done so that the luminous flux at each segment remains the same.

When the initial distribution is carefully analyzed, it is clear that the segments that are shown in turquoise (segment 1 and segment 6) require substantial improvement as there is almost no flux in the region. The luminous flux in the segments represented in red (3 and 4) has to be redirected away as it constitutes more luminous flux than required. By using the shift and scan technique, the grid points that got mapped to segments 1 and 6 are identified and given to the OFFD as the optimization variables in the next step. Based on the selected grid points, optimization is carried out using the deviation-based merit function, and the light distribution is examined. In Figure 16B, it is seen that segments 1 and 6 have been improved significantly. The luminous flux at segments 3 and 4 has reduced down to three times because the OFFD has redistributed the luminous flux from these segments to the rest of the segments as expected.

During the optimization process, the manufacturing feasibility analysis tool detected certain surfaces that cannot be manufactured. However, unlike street lighting lens, the hybrid TIR optics has more surfaces, as shown in Figure 15, that are subjected to deformation during each OFFD iteration. However, each surface has different curvature and offset that must be evaluated during the

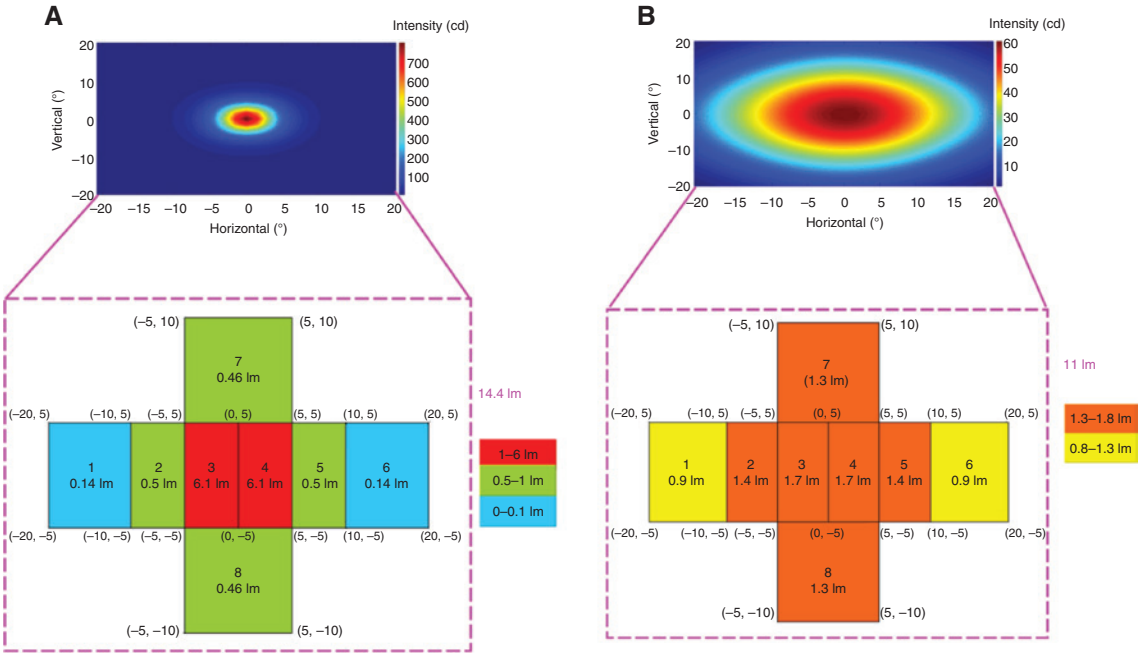

Figure 16: Intensity distribution of the stop lamp with the target being split into eight segments showing the flux contribution at each segment: (A) initial TIR hybrid optics and (B) optimized TIR hybrid optics showing improved luminous flux in each segment satisfying the ECE legal requirements.

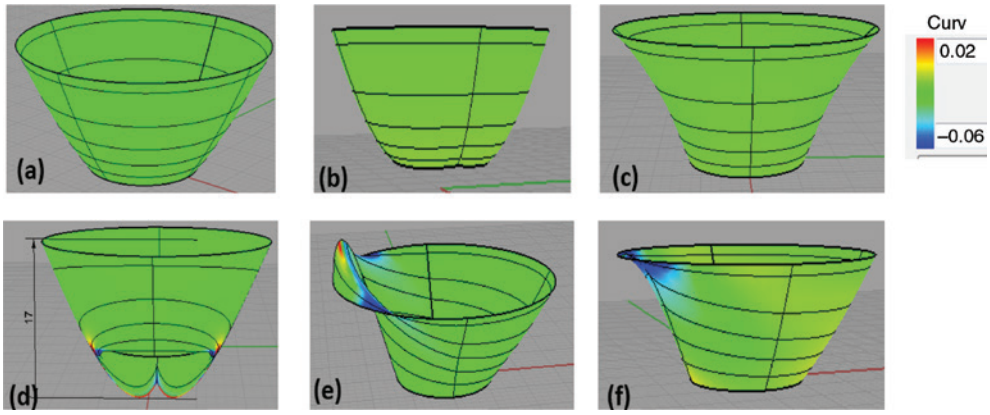

Figure 17: Examples of deformed TIR surfaces for the stop lamps detected by the intelligent OFFD during the manufacturing feasibility analysis.

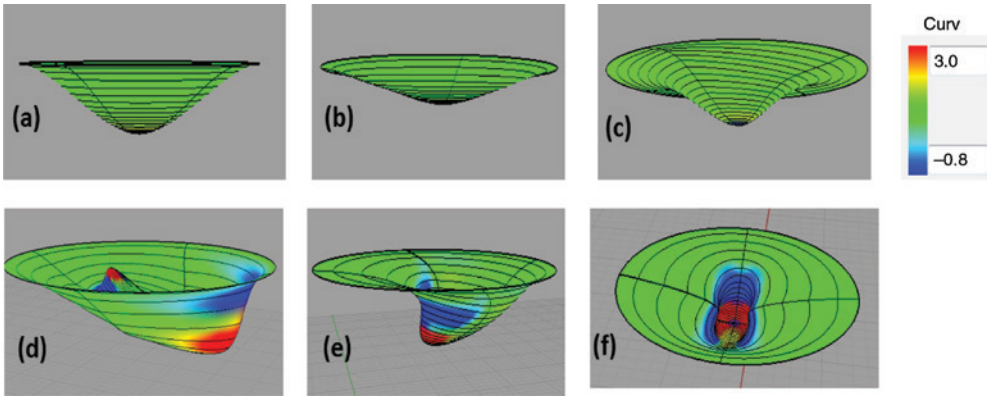

Figure 18: Examples of deformed refracting surfaces for the stop lamps detected by the intelligent OFFD during the manufacturing feasibility analysis.

optimization. So every surface is analyzed individually whether the curvature or its size exceeds the threshold. If it is within the limit, the optimization continues further, or else, it re-iterates back. As seen in Figure 17, the TIR surface undergoes deformation, and the optical surfaces in (A) to (C) are feasible to manufacture. The surfaces in (D) to (F) are infeasible surfaces as they exceed the tolerance limit. Some examples of refracting surfaces are shown in Figure 18. As expected, the tool identified the infeasible surfaces (Figure 18D–F) when the curvature or size reaches its threshold.

As a second step, the deformed surface has to be optimized again to distribute the luminous flux to the outer edges, –15° until +15° vertically and –45° until 45° horizontally. After sufficient optimization and reiteration, the intensities at all the test points fulfill the ECE standard [18] as shown in Table 2. The total luminous flux redirected to the high-intensity region (–5° until +5° vertically and –10° until 10° horizontally) came around 11 lumens, and the remaining 4 lumens have been utilized for the outer edges with the total optical efficiency of the TIR hybrid optics at around 93.5%. The optics obtained as a result of the full automated intelligent OFFD (magenta) along with the initial TIR optics (as turquoise) are overlapped together as shown in Figure 19.

8 Conclusion

In this contribution, two important techniques have been implemented and validated. As a first implementation, the relationship between the light distribution and the optical surface is established using the shift and scan technique. This approach is efficient compared to any traditional optimization algorithm where the entire distribution is evaluated using a single numerical value. By this new implementation, the optimization gained more control on the surface modification as its impact is quantified at specified locations in the target. This mapping helped to select optimal grid points for the optimization

Table 2: Luminous Intensity at test points with ECE values (shown in black), initial and optimized results with failed values marked as red and passed values marked in green.

	[deg]	–45°	–30°	–20°	–10°	–5°	0°	5°	10°	20°	30°	45°
ECE initial optimized	15°	0.3	0.3	0.3	0.3	0.3	0.3	0.3	0.3	0.3	0.3	0.3
		0.08	0.05	1	3	4	4	4	3	1	0.05	0.08
		0.6	0.75	3	12	19	21	19	12	3	0.75	0.6
	10°	0.3	–	–	–	12	12	12	–	–	–	0.3
		0.1				9.5	14	9.5				0.1
		0.45				37	40	37				0.45
	5°	0.3	–	6	12	–	42	–	12	6	–	0.3
		0.1		3	9		156		9	3		0.1
		0.45		14	39		55		39	14		0.45
	0°	0.3	–	–	21	54	60	54	21	–	–	0.3
		0.1			15	156	810	156	15			0.1
		0.5			45	57	64	57	45			0.5
	–5°	0.3	–	6	12	–	42	–	12	6	–	0.3
		0.1		3	9		156		9	3		0.1
		0.45		14	39		55		39	14		0.45
	–10°	0.3	–	–	–	12	12	12	–	–	–	0.3
		0.1				9.5	14	9.5				0.1
		0.45				37	40	37				0.45
	–15°	0.3	0.3	0.3	0.3	0.3	0.3	0.3	0.3	0.3	0.3	0.3
		0.08	0.05	1	3	4	4	4	3	1	0.05	0.08
		0.6	0.75	3	12	19	21	19	12	3	0.75	0.6

The obtained light distribution has passed the UNECE R7 S1 [18] at all the test points.

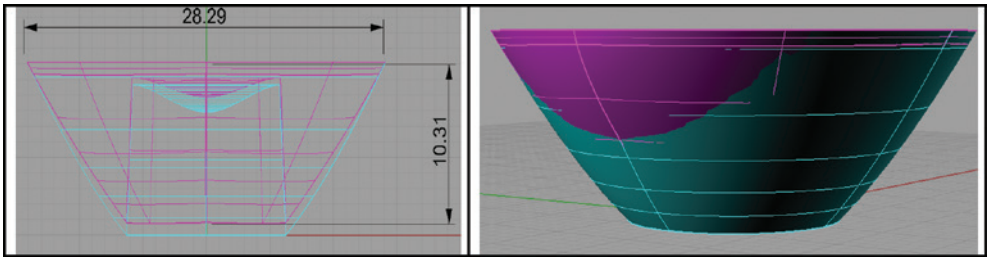

Figure 19: The optics obtained as a result of the full automated intelligent OFFD (magenta) along with the initial TIR optics (as turquoise) are overlapped together.

algorithm. The second one is the implementation of manufacturing feasibility analysis to the OFFD. Ray tracing was performed only for the surfaces feasible to manufacture, thereby, eliminating the unnecessary ray traces, which enhanced the speed of the system. These techniques were implemented in such a way that the intelligent OFFD could replace the optical designer's efforts in terms of his decision making during the process. He needs to specify the target lighting requirements and the initial surface. The OFFD then searches and selects the best possible grid points to be specified as optimization variables to the OFFD. The surface is then optimized using the best grid points during which the quality of the surface is evaluated using the manufacturing feasibility analysis tool, and the photometric and the geometric performances are analyzed using the merit functions. At the end, a deformed surface satisfying the photometric needs and feasible enough to manufacture will be created. These design techniques were verified using two different design requirements.

As a next step, we would like to include the physical limit commonly known as etendue, which describes the attainable target lighting distribution for a particular size and shape of the optics. Then, this distribution can be fed into the OFFD system. This further accelerates the speed as the optimization is directed to obtain a physically attainable light distribution than searching a non-attainable solution.

References

[1] H. Ries and J. Muschaweck, JOSA A 19, 590–595 (2002).
[2] A. S. Isaac and C. Neumann, Proc. SPIE 9889, 98890X (2016).
[3] P. Gimenez-Benitez, J.C. Miñano, J. Blen, R. Mohedano Arroyo, and J. Chaves, et al., Opt. Eng. 43, 1489–1502 (2002).
[4] F. Fournier, W. J. Cassarly and J. P. Rolland, Opt. Express 18, 5295–5304 (2010).
[5] R. J. Koshel, 'Illumination Engineering: Design with Non-Imaging Optics', (John Wiley and Sons, Tucson, Arizona, USA, 2012).
[6] W. J. Cassarly and M. J Hayford, in 'International Society for Optics and Photonics', (2002) pp. 258–269.
[7] S. Kudaev and P. Schreiber, Proc. SPIE 6342, 0353 (2007) .
[8] S. Wendel, J. Kurz and C. Neumann, Proc. SPIE 8550, 85502T (2012).
[9] T. W. Sederberg and S. R. Parry, ACM SIGGRAPH Computer Graphics 20, 151–160 (1986).
[10] J. A. Nelder and R. Mead, Comput. J. 7, 308–313 (1965).
[11] S. Wendel, 'Freiform-Optiken im Nahfeld von LEDs', (KIT Scientific Publishing, Karlsruhe, Germany, 2014) 7, pp. 103–165.
[12] H. Hagen, S. Hahmann and T. Schreiber, Comput. Aided Des. 27, 545–552 (1995).
[13] A. N. Pressley, 'Elementary Differential Geometry', (Springer Science and Business Media, London, UK, 2010).
[14] S. Musuvathy, J.-K. Seong and E. Cohen, Comput. Aided Des. 43, 756–770 (2011).
[15] L. Mohammed and G. Al-Kindi, Eng. Technol. J. 24, 844–852 (2005).
[16] L. Piegl and W. Tiller, 'The NURBS Book', (Springer-Verlag Berlin Heidelberg, 2012).
[17] Product Family Datasheet: 2012. CREE XLamp XP-G2 LEDs, CREE.
[18] UN Vehicle Regulations – 1958 Agreement. 2012. Uniform provisions concerning the approval of front and rear position lamps, stop-lamps and end-outline marker lamps for motor vehicles and trailers. Addendum 6, Regulation No.7.
[19] Product Family Datasheet: 2015. LUXEON Rebel LEDs, Philips LUMILEDS.